catalysts

MDPI

Article

Highly Active Rutile TiO_2 for Photocatalysis under Violet Light Irradiation at 405 nm

Fumiaki Amano [1,*], Akira Yamamoto [2] and Jun Kumagai [3]

[1] Department of Applied Chemistry for Environment, Graduate School of Urban Environmental Sciences, Tokyo Metropolitan University, 1-1 Minami-Osawa, Hachioji, Tokyo 192-0397, Japan
[2] Department of Interdisciplinary Environment, Graduate School of Human and Environmental Studies, Kyoto University, Yoshida-Nihonmatsu-cho, Sakyo-ku, Kyoto 606-8501, Japan
[3] Institute of Materials and Systems for Sustainability, Division of Materials Research, Nagoya University, Furo-cho, Chikusa-ku, Nagoya 464-8603, Japan
* Correspondence: f.amano@tmu.ac.jp

Abstract: Anatase TiO_2 is a widely investigated photocatalyst; however, it can only work under ultraviolet (UV) light with wavelengths less than 390 nm (band gap 3.2 eV). Rutile TiO_2 can absorb visible light at wavelengths less than 410 nm (band gap 3.0 eV); however, its photocatalytic activity is not high. Herein, we activated rutile TiO_2, which was prepared from Evonik TiO_2 P 25 through calcination at 800 °C using hydrogen reduction treatment at 700 °C. The photocatalytic activity of the hydrogen-treated TiO_2 was as high as P 25 under UV irradiation at 380 nm, which was significantly higher than P 25 under violet light irradiation at 405 nm for the oxidative decomposition of acetic acid in water. Electron spin resonance studies indicate that charge separation is enhanced in reduced TiO_2, and their oxygen reduction pathways differ between anatase and rutile. The formation of H_2O_2 was observed on rutile TiO_2; however, it was consumed during photocatalysis to accelerate acetic acid decomposition.

Keywords: blue titania; electron paramagnetic resonance; ESR; hydrogen peroxide; mineralization; oxygen reduction reaction; titanium dioxide; Ti^{3+} species; visible light

Citation: Amano, F.; Yamamoto, A.; Kumagai, J. Highly Active Rutile TiO_2 for Photocatalysis under Violet Light Irradiation at 405 nm. *Catalysts* **2022**, *12*, 1079. https://doi.org/10.3390/catal12101079

Academic Editor: Da-Ren Hang

Received: 5 September 2022
Accepted: 17 September 2022
Published: 20 September 2022

1. Introduction

Titania (TiO_2) is one of the most investigated photocatalytic materials for the environmental purification of air and water under ultraviolet (UV) light irradiation [1–4]. There are several studies on the photocatalytic activity of anatase TiO_2 for the oxidative decomposition of organic pollutants in air and water. In contrast, rutile TiO_2 has not been extensively studied due to the lower photocatalytic activity in the presence of O_2 as an oxidizing species [5–7]. However, rutile can be effectively used in photocatalytic applications because it can absorb violet light in the visible region owing to the band gap energy (E_g = 3.0 eV, onset wavelength λ_{onset} = 413 nm) being narrower than that of anatase (E_g = 3.2 eV, λ_{onset} = 388 nm) [3,8].

High photocatalytic activities are frequently reported for anatase TiO_2 with a high specific surface area [3,9]. Anatase TiO_2 irreversibly transforms into rutile, which is in a thermodynamically stable phase, through high-temperature calcination (Figure 1a). However, this heat treatment at high temperatures decreased the specific surface area due to the increase in the particle size and decreased photocatalytic activity. The surface OH groups also decreased under thermal treatment. The decrease in surface OH group density has been correlated with the lower photocatalytic activity of TiO_2 [5,10,11].

The low photocatalytic activity of rutile TiO_2 is also explained by the energy level of the conduction band minimum (CBM) of rutile, which is less than that of anatase (Figure 1b) [5]. Electrochemical studies indicate that the flat band potential, which is located just under the CBM for an n-type semiconductor, of rutile TiO_2(001) is more positive than that of

anatase TiO_2(101) by 0.2 V [8]. This may affect the electron transfer to oxygen, which is the rate-determining process in photocatalysis [12–14]. The position of the CBM of rutile implies that a one-electron reduction in O_2 with conduction band electrons (e_{cb}^-) to form superoxide radical anions ($O_2^{\bullet-}$) may be difficult to achieve in rutile (Figure 1b).

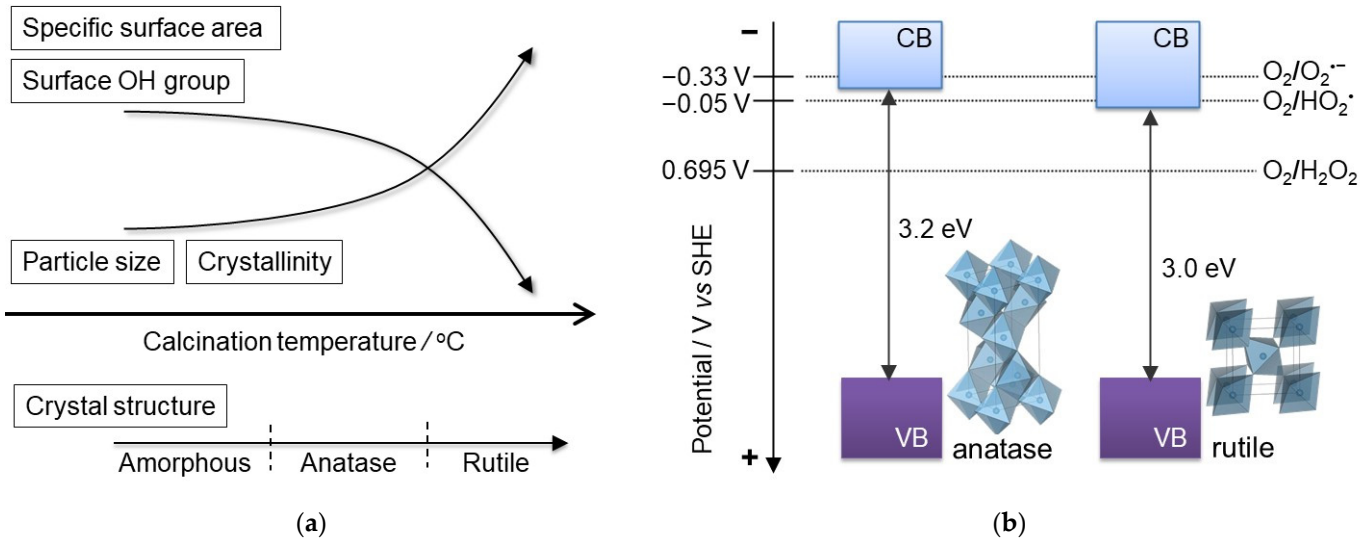

Figure 1. (**a**) Effect of calcination temperature on the properties of TiO_2. (**b**) Schematic energy diagram of anatase and rutile TiO_2 and the standard electrode potentials for the oxygen reduction reaction. The conduction band (CB) minimum positions were assumed from the reported flat band potentials, and the valence band (VB) maximum positions were derived from their band gap energies.

In addition, several reports have concluded that the recombination of photogenerated carriers is likely to occur in rutile TiO_2 [15–17]. The electron mobility of rutile is less than that of anatase [18,19]. The difference in the depth of electron traps has also been elucidated by time-resolved visible and infrared absorption spectroscopies [15].

Nevertheless, it has been revealed that H_2 reduction treatment improves the photocatalytic and photoelectrochemical activities of rutile TiO_2 [20–26]. However, the application of H_2-treated rutile TiO_2 has been limited for photocatalytic oxidative decomposition of organic compounds since it is believed that rutile is not active for photocatalysis with oxygen reduction. In this study, we investigated the photocatalysis of H_2-treated rutile TiO_2 for the mineralization of acetic acid to carbon dioxide (CO_2). Acetic acid is one of the most studied model compounds for the photocatalytic mineralization of organic pollutants and intermediates during the oxidative decomposition of acetaldehyde. Herein, we firstly found that the H_2-treated rutile TiO_2 exhibited high photocatalytic activity for the oxidative decomposition reaction even under violet light irradiation (405 nm). We explored the mechanism for enhanced photocatalytic activity using electron spin resonance (ESR) spectroscopy and quantification of hydrogen peroxide (H_2O_2) during the photocatalytic reactions.

2. Results

2.1. Preparation and Characterization

We used Evonik/Degussa Aeroxide® P 25, which is a commercial TiO_2 with high photocatalytic activity [27], with varying compositions of anatase (~85%) and rutile (~15%) [28]. P 25 powder was calcined in air at 800 °C for 2 h. Thus-obtained P800 was further treated with H_2 flow at 700 °C for 2 h. The H_2-treated TiO_2 is denoted as P800-H700.

Figure 2 shows the scanning electron microscope (SEM) images of the TiO_2 samples. The particle size increased from ~30 to ~100 nm after calcination. In contrast, the hydrogen treatment did not change the particle size of P800. These phenomena were supported by the BET-specific surface areas (SSA_{BET}), which were 55, 9.6, and 9.8 $m^2\ g^{-1}$ for P 25, P800, and P800-H700, respectively.

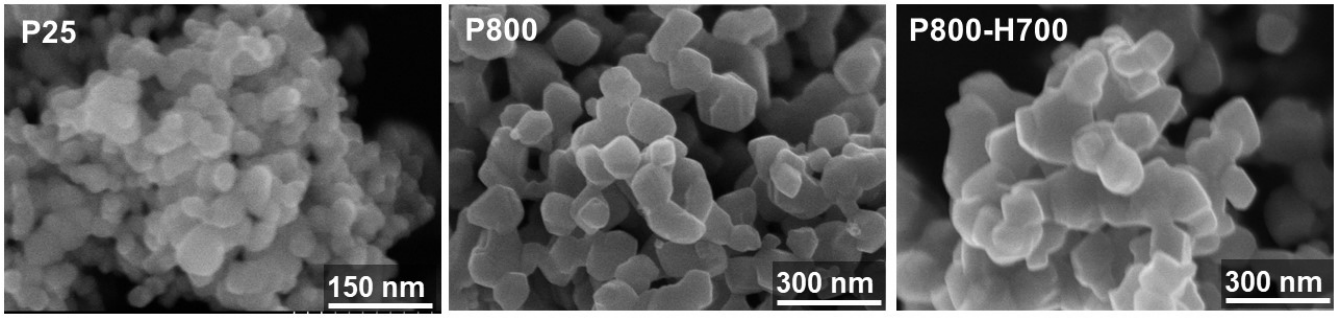

Figure 2. FE-SEM images of TiO_2 particles (P 25, P800, and P800-H700).

Figure 3 shows powder X-ray diffraction (XRD) patterns of TiO_2 with nickel oxide, which was added to 30 wt% as an internal standard. P 25 was composed of anatase (87%) and rutile (13%) [24,29]. Calcination at 800 °C converted anatase to pure rutile (100%). P800-H700 also consisted of a single phase of rutile TiO_2.

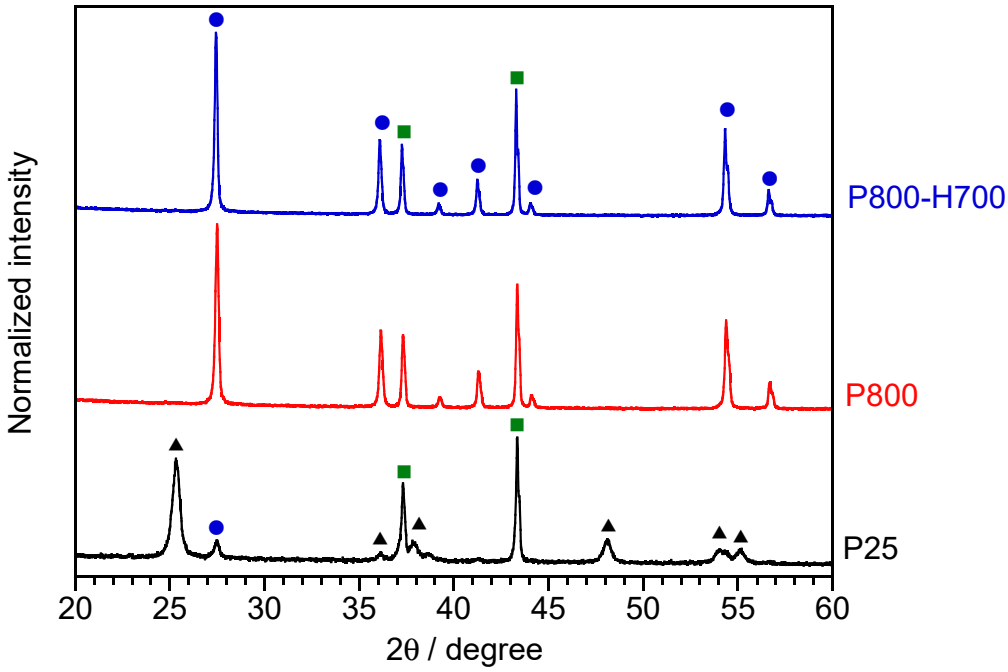

Figure 3. XRD patterns of TiO_2 powders mixed with NiO as an internal standard: (●) Rutile TiO_2, (▲) anatase TiO_2, and (■) NiO.

2.2. Optical Properties of TiO_2 Particles

Figure 4a shows the diffuse reflectance UV-visible spectra using barium sulfate as a reference. The optical absorption onset (λ_{onset}) of P 25 was exhibited at ~410 nm, which is consistent with 3.02 eV of rutile TiO_2. However, the absorption edge of P 25 was not steep because rutile was not the major phase in P 25. P800 and P800-H700 exhibited steeper absorption edges than P 25. The λ_{onset} of P800 and P800-H700 was ~415 nm (2.99 eV), which is consistent with the E_g of rutile TiO_2 [8,30,31].

As shown in Figure 4b, P800 was white, whereas P800-H700 was pale blue. This blue color is related to visible light absorption. The 1—reflectance values at wavelengths longer than 420 nm were not zero for all samples. However, the values of P 25 and P800 originate from scattering. In contrast, the extinction of P800-H700 is attributed to electron transitions from the shallow traps in Ti^{3+}-enriched TiO_2 [32–34]. The blue TiO_2 implies the formation of partially reduced TiO_2 with Ti^{3+} species.

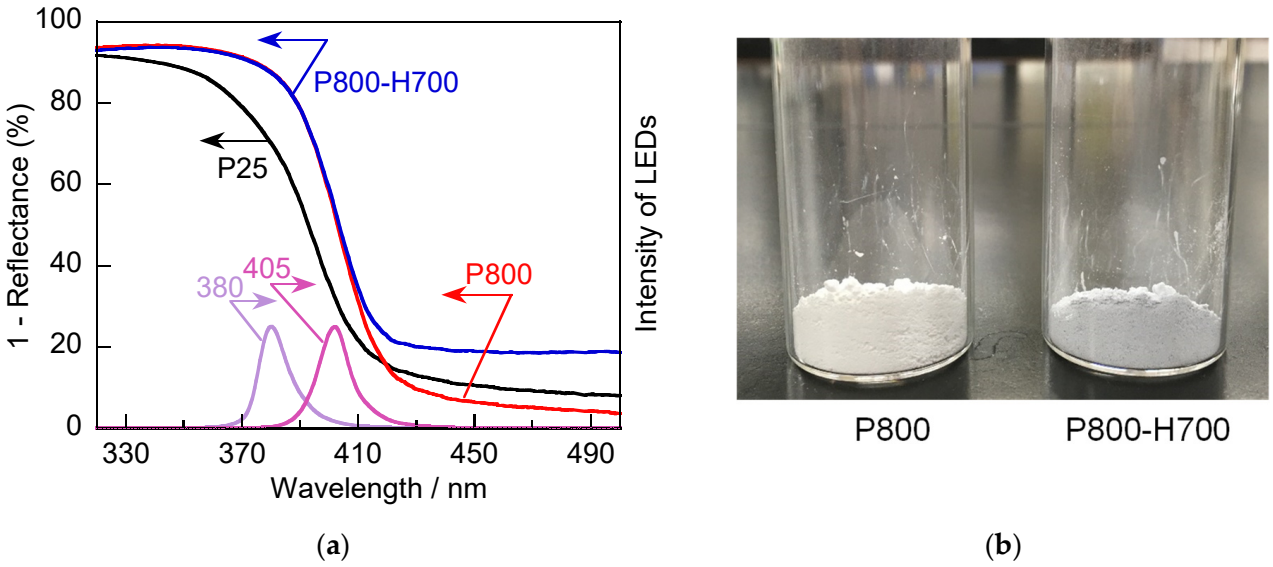

Figure 4. (**a**) Diffuse reflectance UV-visible spectra of TiO_2 samples and emission spectra of 380 and 405 nm light-emitting diodes (LEDs) used for photocatalytic reaction. (**b**) Photograph of TiO_2 powders: P800 and P800-H700.

2.3. Photocatalytic Activity Test

Figure 5 shows the time course of photocatalytic CO_2 evolution through the decomposition of acetic acid in water. CO_2 evolution was effectively induced by the highly active P 25 and P800-H700 under UV illumination at 380 nm. In contrast, CO_2 evolution over P800 was sluggish because of the phase transformation to rutile. The decreased activity may be explained by the decrease in the specific surface area. However, P800-H700 with low SSA_{BET} (9.8 m^2 g^{-1}) also exhibited high activity, which is comparable to that of highly active P 25 (SSA_{BET} = 55 m^2 g^{-1}). This implies that the intrinsic activity per unit surface area was significantly high for H_2-treated rutile TiO_2.

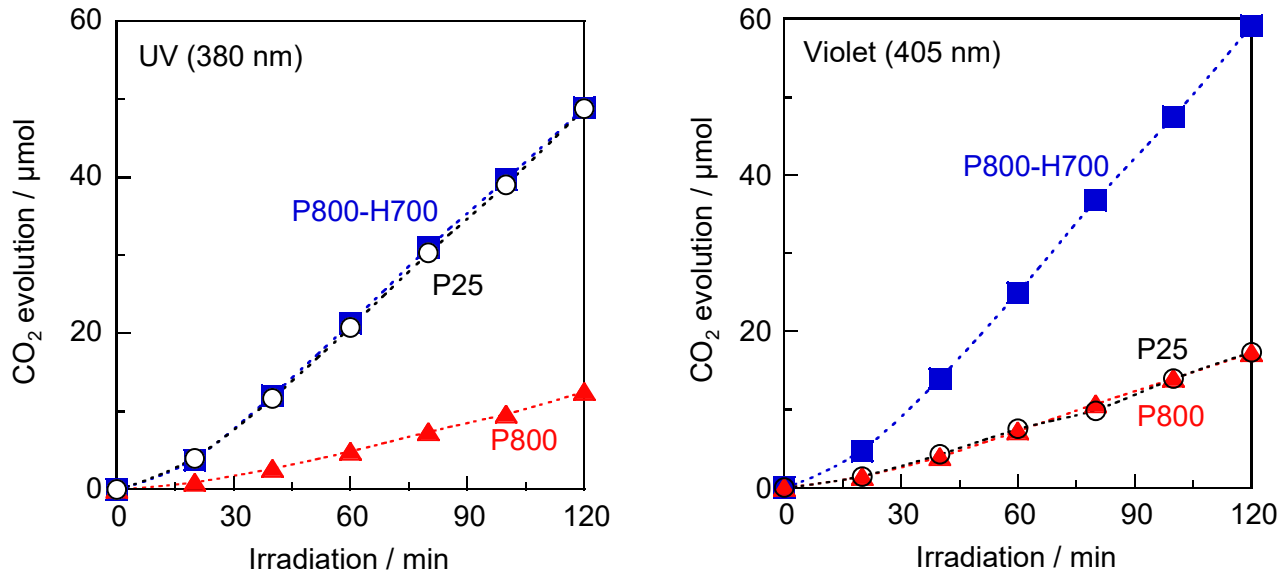

Figure 5. Photocatalytic CO_2 evolution through oxidative decomposition of acetic acid under (**a**) 380-nm UV irradiation (9 mW cm^{-2}) and (**b**) 405-nm violet light irradiation (18 mW cm^{-2}). Photocatalyst: 50 mg, liquid phase: 1 vol% CH_3COOH aq. (9.0 mL), gas phase: Oxygen (15 mL), and temperature 25 °C.

Figure 5b shows the results of the photocatalytic reaction under violet light at 405 nm. In this visible light region, the photocatalytic activity of P 25 was very low because the

main component of anatase could not absorb violet light. The CO_2 evolution of P 25 was as low as P800 under 405-nm irradiation. In contrast, P800-H700 exhibited significantly higher photocatalytic activity than anatase-rich P 25 and conventional rutile TiO_2. Rutile can absorb violet light; however, its photocatalytic activity is generally less than that of anatase. However, H_2-treated rutile exhibited high photocatalytic activity even in the violet light region. The apparent quantum efficiencies of CO_2 evolution were 8.4% at 380 nm and 4.9% at 405 nm when four electrons were required for one molecule of CO_2 formation ($CH_3COOH + 2H_2O \rightarrow 2CO_2 + 8H^+ + 8e^-$).

2.4. ESR Study

To determine the reason for the enhanced activity, we measured the ESR spectra of H_2-reduced rutile (Figure 6). The signal assigned to the Ti^{3+} species at g = 2.0–1.8 was not observed for P800. In contrast, P800-H700 exhibited a broad signal of Ti^{3+} at g = 2.0–1.8. The signal at $g\perp$ = 1.97 is assigned to Ti^{3+} in rutile TiO_2 [35,36]. The signal broadening in H_2-reduced TiO_2 suggests a magnetic dipole–dipole interaction due to the high density of Ti^{3+} species [34].

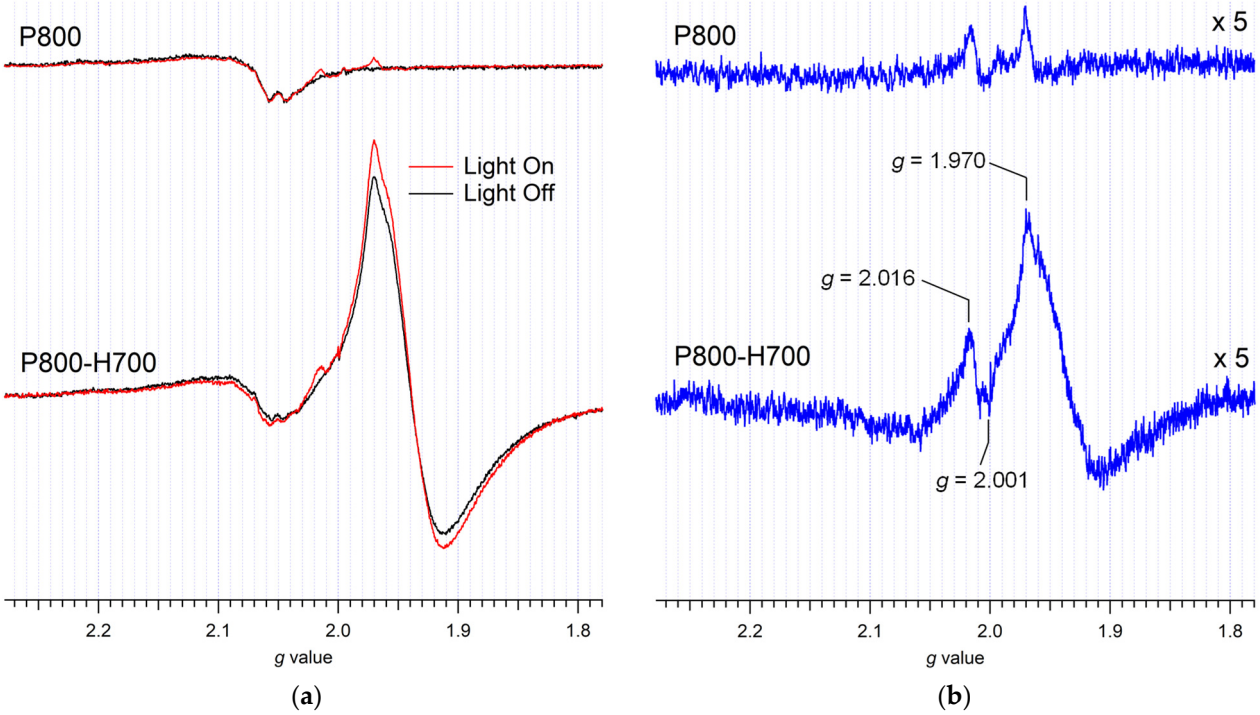

Figure 6. (**a**) ESR spectra of P800 and P800-H700 with helium (18 Torr) at −253 °C. (**b**) Difference spectra between before and after UV irradiation at 365 nm.

When the sample was exposed to UV light, the signal changed slightly. The different spectra before and after UV irradiation indicate an increase in Ti^{3+} and the formation of photogenerated holes trapped on the lattice oxygen atom ($O_L^{\bullet-}$) with g values in the range of 2.02–2.00. The increment in the signal intensities was higher for P800-H700 than for P800, suggesting more efficient charge separation in H_2-reduced rutile TiO_2 under UV irradiation. The longer lifetime of the trapped electrons indicates the high activity of P800-H700.

We further investigated the oxygen reduction reaction over anatase and rutile TiO_2 using ESR spectroscopy (Figure 7). After evacuation, P 25 exhibits a signal at g = 1.98, which is assigned to the Ti^{3+} in anatase TiO_2 [35,36]. A signal intensity less than that of P800-H700 indicates the low density of T^{i3+} in P 25. In the presence of molecular oxygen (1.0 Torr), there are several signals of paramagnetic O_2 exhibited in the gas phase (Figure S1 in the Supplementary Materials) [37]. Under UV irradiation, P 25 exhibited signals at g = 2.04–1.98. The line shape was not resolved and was superimposed on several

radicals. The superoxide anion ($O_2^{\bullet-}$) on anatase can be identified as g_1 = 2.020–2.029, g_2 = 2.009, and g_3 = 2.003 [38–43]. When photogenerated e_{cb}^- is used for O_2 reduction, the valence band hole is trapped on the surface ($O_L^{\bullet-}$). The g-values of $O_L^{\bullet-}$ in anatase were g_1 = 2.016, g_2 = 2.012, and g_3 = 2.002 [35,38,39]. Therefore, we assigned the unresolved signals to $O_2^{\bullet-}$ and $O_L^{\bullet-}$ to anatase. However, the $O_2^{\bullet-}$ signal was not formed for P800-H700, even under UV irradiation. The weak and broad signal at g = 2.015 can be assigned to $O_L^{\bullet-}$ on rutile. The absence of the $O_2^{\bullet-}$ signal suggests that a one-electron reduction pathway ($O_2 + e_{cb}^- \rightarrow O_2^{\bullet-}$) does not occur in Ti^{3+}-rich rutile (P800-H700). A similar result was reported for the Bi_2WO_6 photocatalyst [44].

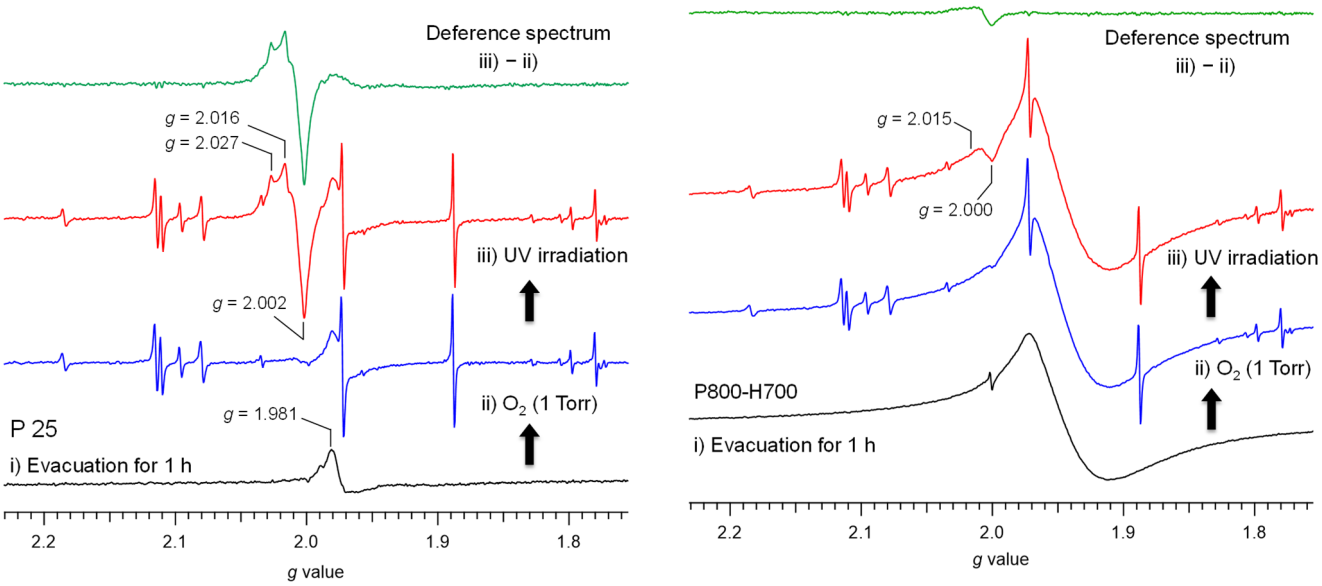

(**a**) (**b**)

Figure 7. ESR spectra at −150 °C of (**a**) P 25 and (**b**) P800-H700. The sample was measured after (i) evacuation at 25 °C for 1 h, (ii) introduction of 1.0 Torr of oxygen, and (iii) UV irradiation with oxygen. The difference spectra between before and after photoirradiation are also shown.

2.5. Effect of H_2O_2 Addition on the Photocatalytic Activity

The fact that one-electron oxygen reduction was not involved in the photocatalysis of rutile TiO_2 motivated us to confirm the presence of a two-electron pathway ($O_2 + 2H^+ + 2e_{cb}^- \rightarrow H_2O_2$). Table 1 summarizes the formation of H_2O_2 during the photocatalytic reaction of acetic acid decomposition. H_2O_2 was analyzed by the colorimetric method using the oxidation of iodide to triiodide ions (Equations (1) and (2)) [45–47].

$$H_2O_2 + 2H^+ + 2I^- \rightarrow 2H_2O + I_2 \quad (1)$$

$$I_2 + I^- \rightarrow I_3^- \quad (2)$$

Table 1. Photocatalytic reaction in 1 vol% CH_3COOH aqueous solution after violet light irradiation for 20 min.

Photocatalyst	Formed H_2O_2/μmol	Evolved CO_2/μmol
P 25	0.17	1.19
P800	0.03	0.88
P800-H700	0.09	3.36
blank	–	0.00

We confirmed that H_2O_2 was formed in the photocatalytic reaction over 20 min; however, the formed amount was significantly low for P800-H700 (Table 1). Because H_2O_2 is easily decomposed, we investigated the degradation behavior of H_2O_2 under photocatalytic conditions. Table 2 summarizes the effect of the presence of 9 μmol of H_2O_2 in the feed. Without TiO_2 photocatalysts, H_2O_2 did not decompose even under light irradiation. In contrast, the added H_2O_2 did not remain after 20 min of photocatalysis over Ti^{3+}-rich rutile TiO_2. This fast degradation can explain the low amount of H_2O_2 formed during the photocatalytic reaction. Notably, CO_2 evolution was significantly enhanced by the H_2O_2 addition for P800-H700. This suggests that H_2O_2 promotes the decomposition of acetic acid over the Ti^{3+}-rich rutile TiO_2.

Table 2. Photocatalytic reaction in 1 vol% CH_3COOH aqueous solution with 9 μmol H_2O_2 after violet light irradiation for 20 min.

Photocatalyst	Residual H_2O_2/μmol	Evolved CO_2/μmol
P 25	2.93	0.89
P800	1.48	2.39
P800-H700	0.03	8.60
blank	9.39	0.00

3. Discussion

The flat band potential of rutile TiO_2 is reported to be +0.05 or +0.13 V vs. the standard hydrogen electrode (SHE) [30,31]. The flat band potential of anatase is more negative than that of rutile TiO_2 by 0.20–0.26 eV [8,48]. Thus, the CBM of anatase and rutile is roughly assumed to be located at approximately −0.2 and 0 V vs. SHE, respectively (Figure 1b). To reduce oxygen, the CBM should be more negative than the standard electrode potentials of the oxygen reduction reactions, as expressed in Equations (3)–(5) [49].

$$O_2 + e^- = O_2^{\bullet -}, E^\circ = -0.33 \text{ V vs. SHE} \quad (3)$$

$$O_2 + H^+ + e^- = HO_2^\bullet, E^\circ = -0.046 \text{ V vs. SHE} \quad (4)$$

$$O_2 + 2H^+ + 2e^- = H_2O_2, E^\circ = +0.695 \text{ V vs. SHE} \quad (5)$$

As shown in Figure 1, the CBM of anatase is close to or more negative than the thermodynamic theoretical potential for one-electron reduction to form oxygen radicals ($O_2^{\bullet -}$ and $HO_2^\bullet$). In contrast, the CBM of rutile TiO_2 cannot promote one-electron reduction, as demonstrated by ESR. Nevertheless, two-electron reduction of oxygen is thermodynamically possible for rutile. In addition, the formation of H_2O_2 during the photocatalytic reaction was confirmed (Table 1). H_2O_2 formation has also been reported in Pt-WO_3 and Bi_2WO_6 photocatalysts with deep CBM [46,47,50].

The low amount of H_2O_2 during photocatalysis can be explained by the rapid degradation by the e_{cb}^- in the rutile photocatalyst, as expressed in Equation (6) [46,49].

$$H_2O_2 + e^- = {}^\bullet OH + OH^-, E^\circ = +1.14 \text{ V vs. SHE} \quad (6)$$

The in situ-generated H_2O_2 can act as an electron scavenger to retard the recombination of photogenerated carriers [50]. The reaction of e_{cb}^- with H_2O_2 is easier than with O_2. Moreover, the hydroxyl radical ($^\bullet OH$) formed is a very strong oxidant (E° = +2.38 V vs. SHE), thus promoting acetic acid degradation [5,10,51]. This hypothesis agrees with the enhanced CO_2 formation by adding H_2O_2 (Table 2).

Figure 8 illustrates the proposed reaction scheme for a highly active rutile TiO_2 photocatalyst for the oxidative decomposition of acetic acid. It can be observed that charge separation is enhanced in the Ti^{3+}-rich rutile under UV and violet light irradiation (λ < ~415 nm). The photogenerated hole can oxidize acetic acid to the $CH_3COO^\bullet$ radical, which will be $^\bullet CH_3$ radical vis decarboxylation [52]. The two-electron reduction of oxygen by e_{cb}^- is the

plausible pathway in thermodynamics. The formed H_2O_2 retards the recombination and further accelerates the decomposition of acetic acid via radical pathways.

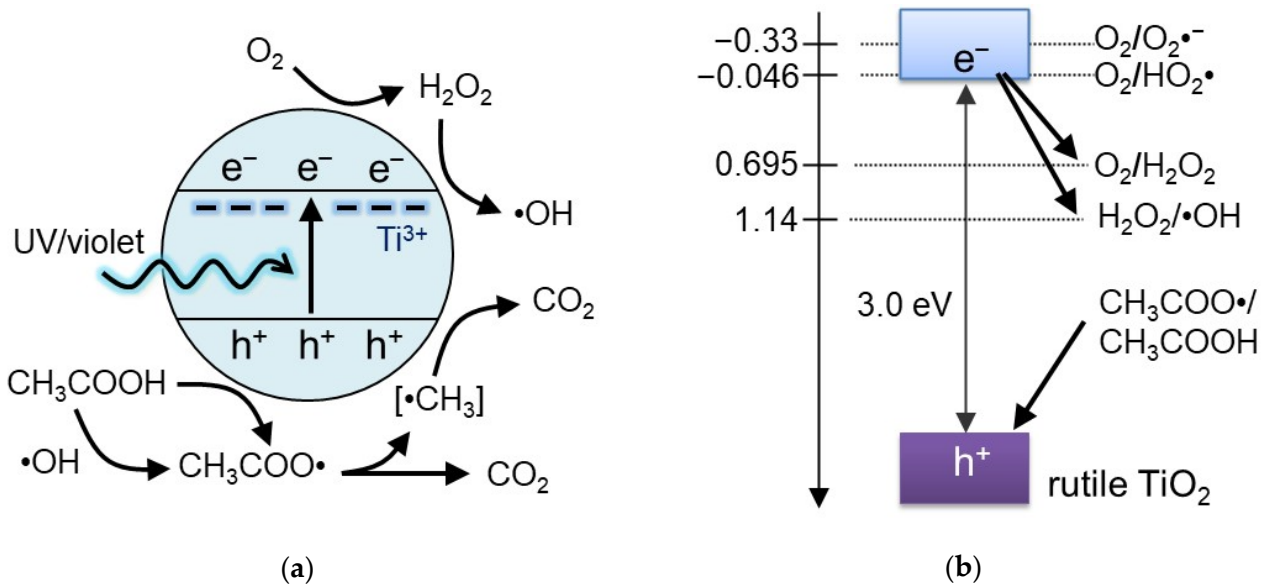

Figure 8. Schematic of the (**a**) proposed reaction mechanism and (**b**) energy diagram for oxidative decomposition of acetic acid by Ti^{3+}-rich rutile TiO_2 photocatalysis.

4. Materials and Methods

Evonik/Degussa Aeroxide TiO_2 P 25 was obtained from Nippon Aerosil Co. (Yokkaichi, Japan). Calcination in air was performed in an alumina crucible in an electric furnace at 800 °C for 2 h. The treatment under H_2 flow (50 mL min^{-1}) was performed in a quartz boat using a quartz tube-type reactor at 700 °C for 2 h. The temperature was naturally cooled to 300 °C under H_2 flow and to room temperature under N_2 flow (100 mL min^{-1}).

SEM images were recorded using a Hitachi S-5200 field emission scanning electron microscope (Tokyo, Japan). The BET-specific surface areas were determined at −196 °C using a MicrotracBEL BELSORP-mini instrument (Osaka, Japan). The XRD patterns were recorded using a Rigaku RINT-2000 diffractometer (Akishima, Japan). UV-visible spectra were obtained using an ALS SEC2000-UV/vis spectrometer (Tokyo, Japan) with a Hamamatsu Photonics L10290 fiber light source (Hamamatsu, Japan).

The photocatalytic activity was examined by measuring CO_2 evolution from an aqueous solution of 1 vol% acetic acid. The reactor was a glass test tube with an outer diameter of 18 mm and the volume of the liquid was 9.0 mL. A suspension of 50 mg TiO_2 particles was sonicated for 1 min and bubbled with oxygen for 5 min. After stirring for 30 min in the dark, photoirradiation was performed using a LED at 25 °C. The evolved CO_2 was detected using a TCD-GC with a Porpak-Q column and helium carrier. The concentration of H_2O_2 was quantified from the UV-visible spectra of I_3^- formed from H_2O_2 (2 mL), 0.2 M KI (1 mL), and 0.2 M H_2SO_4 (1 mL) at 25 °C. The absorbance of I_3^- was measured at 351 nm wavelength.

The ESR spectra were recorded at −253 °C using liquid helium on a JEOL JES-RE1X (Akishima, Japan). The ESR sample tube was irradiated using an ultra-high-pressure mercury lamp with a 365 nm band path filter. A JEOL JES-X320 instrument (Akishima, Japan) was used for the oxygen reduction reaction at −150 °C. UV irradiation was performed using a xenon lamp through a 365 nm band path filter. The samples were pre-evacuated at room temperature for 60 min on a vacuum line before the ESR measurements, and oxygen gas (1.0 Torr) was added to the ESR sample tube at 25 °C.

5. Conclusions

We investigated TiO_2 photocatalysts for the oxidative decomposition of acetic acid to CO_2 under UV and violet light irradiation. Rutile TiO_2 samples were prepared from Evonik TiO_2 P 25 through calcination at 800 °C, followed by H_2 treatment at 700 °C. H_2-treated TiO_2 exhibited high photocatalytic activity, which is comparable to highly active anatase TiO_2, despite its rutile structure and low specific surface area. The high photocatalytic activity under UV irradiation was due to the increase in Ti^{3+} density and the improvement in charge separation, as confirmed by ESR. In the presence of O_2, anatase TiO_2 promoted the formation of $O_2^{\bullet-}$ and $O_L^{\bullet-}$; however, rutile TiO_2 did not exhibit an $O_2^{\bullet-}$ signal. This is because the conduction band edge of rutile is not suitable for the one-electron reduction of oxygen. We observed that the two-electron reduction of O_2 to H_2O_2 was dominant in rutile TiO_2 photocatalysis, and the in situ-formed H_2O_2 accelerated the decomposition of acetic acid. We also found that Ti^{3+}-rich rutile TiO_2 can work even under violet light irradiation (wavelength = 405 nm) owing to its narrower E_g (3.0 eV), and its intrinsic activity per unit surface area is significantly high. The apparent quantum efficiency of H_2-treated TiO_2 for CO_2 evolution was 4.9% at 405 nm, where conventional TiO_2 photocatalysts do not work efficiently.

Supplementary Materials: The following supporting information can be downloaded at https://www.mdpi.com/article/10.3390/catal12101079/s1. Figure S1: ESR spectrum of pure O_2 recorded at −150 °C.

Author Contributions: Investigation and visualization, F.A., A.Y. and J.K.; writing the original draft, F.A. All authors have read and agreed to the published version of the manuscript.

Funding: This research was funded by Japan Society for the Promotion of Science (JSPS KAKENHI) (grant number JP20H02525).

Conflicts of Interest: The authors declare no conflict of interest.

References

1. Hoffmann, M.R.; Martin, S.T.; Choi, W.; Bahnemann, D.W. Environmental applications of semiconductor photocatalysis. *Chem. Rev.* **1995**, *95*, 69–96. [CrossRef]
2. Linsebigler, A.L.; Lu, G.; Yates, J.T. Photocatalysis on TiO_2 surfaces: Principles, mechanisms, and selected results. *Chem. Rev.* **1995**, *95*, 735–758. [CrossRef]
3. Carp, O.; Huisman, C.L.; Reller, A. Photoinduced reactivity of titanium dioxide. *Prog. Solid. State Chem.* **2004**, *32*, 33–177. [CrossRef]
4. Fujishima, A.; Zhang, X.; Tryk, D.A. TiO_2 photocatalysis and related surface phenomena. *Surf. Sci. Rep.* **2008**, *63*, 515–582. [CrossRef]
5. Sclafani, A.; Herrmann, J.M. Comparison of the photoelectronic and photocatalytic activities of various anatase and rutile forms of titania in pure liquid organic phases and in aqueous solutions. *J. Phys. Chem.* **1996**, *100*, 13655–13661. [CrossRef]
6. Hashimoto, K.; Irie, H.; Fujishima, A. TiO_2 photocatalysis: A historical overview and future prospects. *Jpn. J. Appl. Phys* **2005**, *44*, 8269–8285. [CrossRef]
7. Ohno, T.; Sarukawa, K.; Matsumura, M. Photocatalytic activities of pure rutile particles isolated from TiO_2 powder by dissolving the anatase component in HF solution. *J. Phys. Chem. B* **2001**, *105*, 2417–2420. [CrossRef]
8. Kavan, L.; Grätzel, M.; Gilbert, S.E.; Klemenz, C.; Scheel, H.J. Electrochemical and photoelectrochemical investigation of single-crystal anatase. *J. Am. Chem. Soc.* **1996**, *118*, 6716–6723. [CrossRef]
9. Amano, F.; Yasumoto, T.; Prieto-Mahaney, O.O.; Uchida, S.; Shibayama, T.; Ohtani, B. Photocatalytic activity of octahedral single-crystalline mesoparticles of anatase titanium(IV) oxide. *Chem. Commun.* **2009**, *45*, 2311–2313. [CrossRef]
10. Turchi, C.S.; Ollis, D.F. Photocatalytic degradation of organic water contaminants: Mechanisms involving hydroxyl radical attack. *J. Catal.* **1990**, *122*, 178–192. [CrossRef]
11. Du, P.; Bueno-López, A.; Verbaas, M.; Almeida, A.R.; Makkee, M.; Moulijn, J.A.; Mul, G. The effect of surface OH-population on the photocatalytic activity of rare earth-doped P25-TiO_2 in methylene blue degradation. *J. Catal.* **2008**, *260*, 75–80. [CrossRef]
12. Gerischer, H.; Heller, A. The role of oxygen in photooxidation of organic molecules on semiconductor particles. *J. Phys. Chem.* **1991**, *95*, 5261–5267. [CrossRef]
13. Gerischer, H.; Heller, A. Photocatalytic oxidation of organic molecules at TiO_2 particles by sunlight in aerated water. *J. Electrochem. Soc.* **1992**, *139*, 113–118. [CrossRef]
14. Wang, C.M.; Heller, A.; Gerischer, H. Palladium catalysis of O_2 reduction by electrons accumulated on TiO_2 particles during photoassisted oxidation of organic compounds. *J. Am. Chem. Soc.* **1992**, *114*, 5230–5234. [CrossRef]

15. Yamakata, A.; Vequizo, J.J.M.; Matsunaga, H. Distinctive behavior of photogenerated electrons and holes in anatase and rutile TiO_2 powders. *J. Phys. Chem. C* **2015**, *119*, 24538–24545. [CrossRef]
16. Yamada, Y.; Kanemitsu, Y. Determination of electron and hole lifetimes of rutile and anatase TiO_2 single crystals. *Appl. Phys. Lett.* **2012**, *101*, 133907. [CrossRef]
17. Schneider, J.; Matsuoka, M.; Takeuchi, M.; Zhang, J.; Horiuchi, Y.; Anpo, M.; Bahnemann, D.W. Understanding TiO_2 photocatalysis: Mechanisms and materials. *Chem. Rev.* **2014**, *114*, 9919–9986. [CrossRef] [PubMed]
18. Hattori, M.; Noda, K.; Nishi, T.; Kobayashi, K.; Yamada, H.; Matsushige, K. Investigation of electrical transport in anodized single TiO_2 nanotubes. *Appl. Phys. Lett.* **2013**, *102*, 043105. [CrossRef]
19. Luttrell, T.; Halpegamage, S.; Tao, J.; Kramer, A.; Sutter, E.; Batzill, M. Why is anatase a better photocatalyst than rutile?—Model studies on epitaxial TiO_2 films. *Sci. Rep.* **2014**, *4*, 4043. [CrossRef] [PubMed]
20. Amano, F.; Nakata, M.; Asami, K.; Yamakata, A. Photocatalytic activity of titania particles calcined at high temperature: Investigating deactivation. *Chem. Phys. Lett.* **2013**, *579*, 111–113. [CrossRef]
21. Zhen, C.; Wang, L.; Liu, L.; Liu, G.; Lu, G.Q.; Cheng, H.-M. Nonstoichiometric rutile TiO_2 photoelectrodes for improved photoelectrochemical water splitting. *Chem. Commun.* **2013**, *49*, 6191–6193. [CrossRef]
22. Amano, F.; Nakata, M. High-temperature calcination and hydrogen reduction of rutile TiO_2: A method to improve the photocatalytic activity for water oxidation. *Appl. Catal. B* **2014**, *158*, 202–208. [CrossRef]
23. Amano, F.; Nakata, M.; Ishinaga, E. Photocatalytic activity of rutile titania for hydrogen evolution. *Chem. Lett.* **2014**, *43*, 509–511. [CrossRef]
24. Amano, F.; Nakata, M.; Yamamoto, A.; Tanaka, T. Rutile titanium dioxide prepared by hydrogen reduction of Degussa P25 for highly efficient photocatalytic hydrogen evolution. *Catal. Sci. Technol.* **2016**, *6*, 5693–5699. [CrossRef]
25. Amano, F.; Mukohara, H.; Shintani, A. Rutile titania particulate photoelectrodes fabricated by two-step annealing of titania nanotube arrays. *J. Electrochem. Soc.* **2018**, *165*, H3164–H3169. [CrossRef]
26. Amano, F.; Nakata, M.; Vequizo, J.J.M.; Yamakata, A. Enhanced visible light response of TiO_2 codoped with Cr and Ta photocatalysts by electron doping. *ACS Appl. Energy Mater.* **2019**, *2*, 3274–3282. [CrossRef]
27. Ohtani, B.; Mahaney, O.O.P.; Amano, F.; Murakami, N.; Abe, R. What are titania photocatalysts?—An exploratory correlation of photocatalytic activity with structural and physical properties. *J. Adv. Oxid. Technol.* **2010**, *13*, 247–261. [CrossRef]
28. Ohtani, B.; Prieto-Mahaney, O.O.; Li, D.; Abe, R. What is Degussa (Evonik) P25? Crystalline composition analysis, reconstruction from isolated pure particles and photocatalytic activity test. *J. Photochem. Photobiol. A* **2010**, *216*, 179–182. [CrossRef]
29. Spurr, R.A.; Myers, H. Quantitative analysis of anatase-rutile mixtures with an X-ray diffractometer. *Anal. Chem.* **1957**, *29*, 760–762. [CrossRef]
30. Butler, M.A.; Ginley, D.S. Prediction of flatband potentials at semiconductor-electrolyte interfaces from atomic electronegativities. *J. Electrochem. Soc.* **1978**, *125*, 228–232. [CrossRef]
31. Maruska, H.P.; Ghosh, A.K. Photocatalytic decomposition of water at semiconductor electrodes. *Sol. Energy* **1978**, *20*, 443–458. [CrossRef]
32. Yamakata, A.; Ishibashi, T.; Onishi, H. Time-resolved infrared absorption spectroscopy of photogenerated electrons in platinized TiO_2 particles. *Chem. Phys. Lett.* **2001**, *333*, 271–277. [CrossRef]
33. Berger, T.; Anta, J.A.; Morales-Flórez, V. Electrons in the band gap: Spectroscopic characterization of anatase TiO_2 nanocrystal electrodes under Fermi level control. *J. Phys. Chem. C* **2012**, *116*, 11444–11455. [CrossRef]
34. Amano, F.; Nakata, M.; Yamamoto, A.; Tanaka, T. Effect of Ti^{3+} ions and conduction band electrons on photocatalytic and photoelectrochemical activity of rutile titania for water oxidation. *J. Phys. Chem. C* **2016**, *120*, 6467–6474. [CrossRef]
35. Kumar, C.P.; Gopal, N.O.; Wang, T.C.; Wong, M.-S.; Ke, S.C. EPR investigation of TiO_2 nanoparticles with temperature-dependent properties. *J. Phys. Chem. B* **2006**, *110*, 5223–5229. [CrossRef]
36. Hurum, D.C.; Agrios, A.G.; Gray, K.A.; Rajh, T.; Thurnauer, M.C. Explaining the enhanced photocatalytic activity of Degussa P25 mixed-phase TiO_2 using EPR. *J. Phys. Chem. B* **2003**, *107*, 4545–4549. [CrossRef]
37. Seymour, R.C.; Wood, J.C. Paramagnetic gas adsorption. *Surf. Sci.* **1971**, *27*, 605–610. [CrossRef]
38. Howe, R.F.; Gratzel, M. EPR study of hydrated anatase under UV irradiation. *J. Phys. Chem.* **1987**, *91*, 3906–3909. [CrossRef]
39. Nakaoka, Y.; Nosaka, Y. ESR investigation into the effects of heat treatment and crystal structure on radicals produced over irradiated TiO_2 powder. *J. Photochem. Photobiol. A* **1997**, *110*, 299–305. [CrossRef]
40. Okumura, M.; Coronado, J.M.; Soria, J.; Haruta, M.; Conesa, J.C. EPR study of CO and O_2 interaction with supported Au catalysts. *J. Catal.* **2001**, *203*, 168–174. [CrossRef]
41. Coronado, J.M.; Maira, A.J.; Conesa, J.C.; Yeung, K.L.; Augugliaro, V.; Soria, J. EPR study of the surface characteristics of nanostructured TiO_2 under UV irradiation. *Langmuir* **2001**, *17*, 5368–5374. [CrossRef]
42. Carter, E.; Carley, A.F.; Murphy, D.M. Evidence for O_2^- radical stabilization at surface oxygen vacancies on polycrystalline TiO_2. *J. Phys. Chem. C* **2007**, *111*, 10630–10638. [CrossRef]
43. Komaguchi, K.; Maruoka, T.; Nakano, H.; Imae, I.; Ooyama, Y.; Harima, Y. ESR study on the reversible electron transfer from O_2^{2-} to Ti^{4+} on TiO_2 nanoparticles induced by visible-light illumination. *J. Phys. Chem. C* **2009**, *113*, 1160–1163. [CrossRef]
44. Saison, T.; Gras, P.; Chemin, N.; Chanéac, C.; Durupthy, O.; Brezová, V.; Colbeau-Justin, C.; Jolivet, J.-P. New insights into Bi_2WO_6 properties as a visible-light photocatalyst. *J. Phys. Chem. C* **2013**, *117*, 22656–22666. [CrossRef]

45. Klassen, N.V.; Marchington, D.; McGowan, H.C.E. H_2O_2 determination by the I_3^- method and by $KMnO_4$ titration. *Anal. Chem.* **1994**, *66*, 2921–2925. [CrossRef]
46. Tomita, O.; Ohtani, B.; Abe, R. Highly selective phenol production from benzene on a platinum-loaded tungsten oxide photocatalyst with water and molecular oxygen: Selective oxidation of water by holes for generating hydroxyl radical as the predominant source of the hydroxyl group. *Catal. Sci. Technol.* **2014**, *4*, 3850–3860. [CrossRef]
47. Tomita, O.; Otsubo, T.; Higashi, M.; Ohtani, B.; Abe, R. Partial oxidation of alcohols on visible-light-responsive WO_3 photocatalysts loaded with palladium oxide cocatalyst. *ACS Catal.* **2016**, *6*, 1134–1144. [CrossRef]
48. Hengerer, R.; Kavan, L.; Krtil, P.; Grätzel, M. Orientation dependence of charge-transfer processes on TiO_2 (anatase) single crystals. *J. Electrochem. Soc.* **2000**, *147*, 1467. [CrossRef]
49. Bard, A.J.; Parsons, R.; Jordan, J. *Standard Potentials in Aqueous Solution*; CRC Press: Boca Raton, FL, USA, 1985.
50. Sheng, J.; Li, X.; Xu, Y. Generation of H_2O_2 and OH radicals on Bi_2WO_6 for phenol degradation under visible light. *ACS Catal.* **2014**, *4*, 732–737. [CrossRef]
51. Buxton, G.V.; Greenstock, C.L.; Helman, W.P.; Ross, A.B. Critical review of rate constants for reactions of hydrated electrons, hydrogen atoms and hydroxyl radicals ($^{\bullet}OH/^{\bullet}O^-$) in aqueous solution. *J. Phys. Chem. Ref. Data* **1988**, *17*, 513–886. [CrossRef]
52. Kraeutler, B.; Bard, A.J. Heterogeneous photocatalytic synthesis of methane from acetic acid—New Kolbe reaction pathway. *J. Am. Chem. Soc.* **1978**, *100*, 2239–2240. [CrossRef]